J. Chem. Sci. (2020)132:74
https://doi.org/10.1007/s12039-020-01780-7

REGULAR ARTICLE

All-inorganic perovskite $CsPbI_2Br$ as a promising photovoltaic absorber: a first-principles study

PENG XU
Research Institute for Magnetoelectronics and Weak Magnetic-field Detection, College of Science, China Three Gorges University, Yichang 443002, China
E-mail: xupeng@ctgu.edu.cn

MS received 28 September 2019; revised 17 January 2020; accepted 21 January 2020

Abstract. Hybrid organic-inorganic halide perovskites as promising solar cell materials have great concern on their stability. Recently, all-inorganic perovskite $CsPbI_2Br$ has been considered as a first-class alternative with good stability as well as a suitable bandgap, and the highest solar cell efficiency has been achieved up to 16%. Using the first-principles calculations, we found that (i) $CsPbI_2Br$ is stable in tetragonal cell with a direct bandgap of 1.67 eV under PBE functional calculations approximating to the experimental value (1.92 eV). The upper valence band is derived from the antibonding states of s-p coupling, and the CBM is mainly composed of Pb-p states. (ii) The optical absorption is as strong as 10^4 cm^{-1} in the visible light range which can compare to that of the popular halide organic-inorganic hybrid perovskite. (iii) The electron transport material (ETM) in popular perovskite solar cells such as TiO_2, ZnO, SnO_2, PCBM and C_{60} together with the hole transport material (HTM) such as P3HT, CuI, NiO, PTAA and Spiro are suitable for $CsPbI_2Br$ solar cell devices. The band offset between different perovskites demonstrates that it is easier for $CsPbI_2Br$ to be doped p-type than for $CsPbBr_3$ but harder than for $CsPbI_3$.

Keywords. Perovskite; semiconductor; solar cell.

1. Introduction

Hybrid organic-inorganic halide perovskites $APbX_3$ (A = CH_3NH_3 or $CH(NH_2)_2$ and X = Cl, Br or I) have been attracted great attentions[1–4] as they show amazing solar cell performance. Ever since they began to be used as solar cell materials in 2009,[5] now the power conversion efficiency has been achieved above 23%.[6] However, the existence of volatile and hygroscopic organic cations such as CH_3NH_3 (methylammonium) and $CH(NH_2)_2$ (formamidinium) makes the material inevitably suffer from poor stability under heat and humidity conditions[7,8] which becomes a great obstacle toward its large-scale commercialization. The promising alternatives are all-inorganic cesium (Cs)-based perovskites $CsPbX_3$.[9,10] Among these Cs-based perovskites, $CsPbI_3$ has an appropriate bandgap of 1.73 eV,[11,12] but the photovoltaic-active cubic phase suffers from structural instability at room temperature and easily transforms to photovoltaic-inactiveδphase.[13–15] While $CsPbBr_3$ exhibits good stability but has too large bandgap (∼2.3 eV)[10,16] it thus has a limiting absorption in the visible light range. As a trade-off between the phase stability and suitable bandgap, the mixed-halide perovskite $CsPbI_2Br$ has been considered as an optimizing alternative with both good phase stability and tunable bandgap (∼1.92 eV).[17–20] Recently, several $CsPbI_2Br$ based solar cells have been attempted and the highest power conversion efficiency can be already achieved up to above 16%,[21–23] which is the most outstanding among all the Cs-based solar cells. Therefore, the all-inorganic perovskite $CsPbI_2Br$ can be a very promising solar cell material toward industrialization.

Despite the rapid improvement of the solar cell performance, the fundamental physical properties of $CsPbI_2Br$ have not been well-understood. Although the relevant properties of $CsPbI_3$ and $CsPbBr_3$ have been deeply investigated, whether the properties of

*For correspondence

Electronic supplementary material: The online version of this article (https://doi.org/10.1007/s12039-020-01780-7) contains supplementary material, which is available to authorized users.

Published online: 09 June 2020

halide-mixed perovskite $CsPbI_2Br$ are same with that of the $CsPbI_3$ and $CsPbBr_3$ is not well clear. As been well known, the popular perovskites $CsPbI_3$ and $CsPbBr_3$ exhibit superior photovoltaic properties[24–26] such as large band edge dispersion, small carrier effective mass, high light absorption and antibonding character of the upper valence band. In this case, whether the halide-mixed perovskite $CsPbI_2Br$ can inherit all of these superior properties? To address these questions, an investigation on the electronic properties as well as the optical properties becomes very necessary.

Band alignment at the interface is critical for the optimization of the solar cell devices. Proper band alignment can contribute to the rising of the open-circuit voltage (V_{oc}).[27,28] For the perovskite solar cell devices, two most important interfaces are the perovskite/electron transport material (ETM) and perovskite/hole transport material (HTM). The perovskite/ETM interface serves as the electron extraction and perovskite/HTM interface is used to block the electron and transport the hole.[29] Empirically, to facilitate the carrier transport, a suitable perovskite/ETM interface requires that the lowest unoccupied molecular orbital (LUMO) of the ETM should be 0.2 eV lower than the conduction band maximum (CBM) of the perovskite,[30,31] and a suitable perovskite/HTM interface requires that the highest occupied molecular orbital (HOMO) of the HTM should be slightly higher than the valance band minimum (VBM) of the perovskite. The reported state of the art $CsPbI_2Br$ solar cell devices usually use the ETM such as TiO_2 and SnO_2 and HTM such as P3HT, PTAA and Spiro.[21–23,32] How the band alignment of these perovskite/ETM and perovskite/HTM interface has not been clear. Besides TiO_2, SnO_2 and P3HT, there are also several other ETM and HTM that are commonly used in perovskite solar cell devices.[28,31,33] Whether these commonly used ETM and HTM are also suitable for the $CsPbI_2Br$ solar cell devices also should be addressed by their band alignment with $CsPbI_2Br$. Hence, an establishment of the band alignment between the perovskite and the commonly used ETM and HTM will be necessary. Moreover, as the $CsPbI_2Br$ is a halide mixed perovskite between $CsPbI_3$ and $CsPbBr_3$, an understanding of their band edge tuning can also help to understand their tunable physics.

In this paper, through performing first-principles calculations, we have systemically studied the electronic structure, optical properties as well as band alignment and found that (i) the crystal structure of $CsPbI_2Br$ is more likely to be stable in a tetragonal cell with a direct bandgap in the center of Brillouin zone. Same with the case of $CH_3NH_3PbI_3$,[34] the bandgap error of using PBE functional and no spin-orbital coupling (soc) can be nearly cancelled with each other. As a result, the PBE functional calculation can give a reasonable band gap of 1.67 eV approximating to the experimentally measured value ($\sim$1.92 eV). The valance band maximum (VBM) is derived from the antibonding states of hybridization between Pb-s and halide (I and Br)-p orbitals. The conduction band minimum (CBM) is mainly composed of Pb-p states. (ii) The optical absorption of $CsPbI_2Br$ is strong exceeding 10^4 cm^{-1} in the visible light region which can be comparable to that of the popular $CH_3NH_3PbI_3$. (iii) The calculated band alignment shows that the commonly used ETM in popular perovskite solar cells such as TiO_2, ZnO, SnO_2, PCBM and C_{60} together with the HTM such as P3HT, CuI, NiO, PTAA and Spiro are all suitable for $CsPbI_2Br$ solar cell devices. Since the VBM of perovskites $CsPbI_3$, $CsPbBr_3$ and $CsPbI_2Br$ are all derived from the antibonding hybridization between Pb-s and halide-p, and then the Br-4p orbital is lower than the I-5p orbital thereby making the VBM of $CsPbI_2Br$ lower than that of the $CsPbI_3$ but higher than that of the $CsPbBr_3$. While the CBM of them locate at the same height because they are all composed of Pb-p states.

2. Computational

All first-principles calculations are performed under the framework of density functional theory (DFT) as implemented in the vasp code.[35,36] The projected augmented-wave[37,38] pseudopotentials with an energy cutoff of 400 eV for the basis set were employed. The valence electronic configurations for each of the elements $Cs(5s^25p^56s)$, $Pb(5d^{10}6s^26p^2)$, $I(5s^25p^5)$ and $Br(4s^24p^5)$ are adopted. For the exchange-correlation potential, we used the Perdew-Burke-Ernzerhof (PBE) known as PBE.[39] Since the bandgap error underestimated by PBE functional can be nearly cancelled by the error that is overestimated by no-soc calculation, so for saving computational consuming, all the calculations use PBE functional as it can give reasonable results. The k-meshes in $5 \times 5 \times 3$ is used for the bulk calculations and the equivalent k-mesh density is used for the superlattice in simulating the band alignment of interface. All lattice vectors and atomic coordinates were fully relaxed until the Hellmann-Feynman force on each atom is less than 0.01 eV/Å.

3. Results and Discussions

3.1 *Crystal structure*

The cubic $CsPbI_3$ has a desirable bandgap (E_g) of 1.73 eV[11,12] which approximates to the optimal bandgap for light harvesting. However, the $CsPbI_3$ in photovoltaic-active cubic phase is unstable and can spontaneously transform to non-perovskite orthorhombicδphase (E_g = 2.82 eV)[11,12] at room temperature under ambient conditions. $CsPbBr_3$ is a phase-stable orthorhombic perovskite but has too large bandgap (E_g = 2.3 eV)[10,16] for photovoltaic applications. Therefore, mixing the halide anions of $CsPbI_3$ and $CsPbBr_3$ can be a proper method to balance the issues between stability and suitable bandgap. During the formation of $CsPb(I_{1-x}Br_x)_3$ alloy, the Coulomb interaction plays a major role in lowering the formation of energy because of the strong ionic nature of halide perovskites. Yin *et al.,*[40] found that the $CsPb(I_{1-x}Br_x)_3$ alloy could be stable at composition x = 1/3 and x = 2/3 since it can get the largest Coulomb energy gain. As depicted in ref. 40, joint effects of both strain and Coulomb energies, the crystal structure stabilizes at x = 1/3, ie $CsPbI_2Br$. Using structure searching by Monte Carlo simulations based on cluster expansion methods (CEM),[41–44] the atomic structure of such an anion-mixed material $CsPbI_2Br$ with a tetragonal cell has been determined as shown in Figure 1(a). Through our calculations, the total energy per formula of the structure in Figure 1(a) is lower than that of the structure suggested in ref.[45] (see Figure 1(b)) by 58 meV per formula. Therefore, all the calculations in the following will be based on the structure in Figure 1(a). For this structure, after full relaxation, the lattice constant is a = b=8.6 Å, c = 12.9 Å. Since the atomic radii of Br are smaller than that of I, the bonding length of Pb-Br (3.04 Å) is slightly shorter than that of Pb-I (3.23 Å) in the PbI_4Br_2 octahedron.

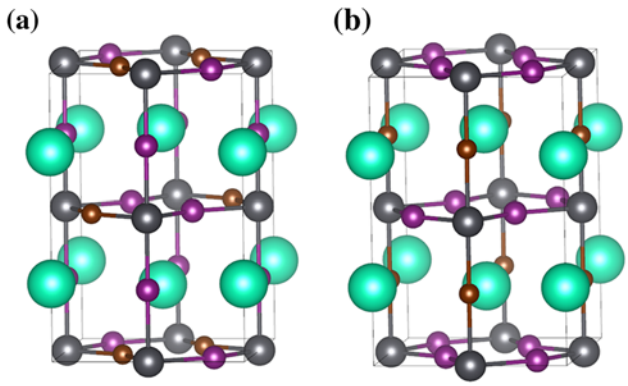

Figure 1. The crystal structure of $CsPbI_2Br$ suggested by ref. 40 (a) and ref. 45 (b). The green, gray, purple and brown balls denote Cs, Pb, I and Br atoms respectively.

3.2 *Electronic structure and optical properties*

The band structure and projected charge density of states of $CsPbI_2Br$ have been shown in Figure 2(a) and (b). Because the PBE band gap error can be nearly cancelled by the error of calculation when no soc effect is considered, so the bandgap given by PBE functional is 1.67 eV approximating to the experimentally measured value (1.92 eV). In the following discussions, all the calculations will use the PBE functional instead of the time-consuming hybrid functional. As seen in Figure 2(a), since the tetragonal cell of the $CsPbI_2Br$ is a supercell of the cubic perovskite cell structure, both VBM and CBM which locate at point R(0.5, 0.5, 0.5) in cubic perovskite[46] fold back to the center of the Brillouin zone (Γ point) in this case. For comparison, the band structures calculated by PBE + soc and hybrid(HSE06[47,48]) + soc functional have been shown in Figure S1 (Supplementary Information). For the projected density of states that are shown in Figure 2(b), similar to the case in $CsPbI_3$ and $CsPbBr_3$, the VBM is mainly derived from the antibonding states of hybridization between Pb-s orbital and the halide (I and Br)-p orbital. The CBM is mainly composed of Pb-p states. Owing to the strong s-p coupling at the upper valence band, the band near the VBM shows a large dispersion thereby demonstrating the $CsPbI_2Br$ would have a superior carrier transport ability.

The light absorption coefficient α(ω)is derived from the dielectric function $\epsilon(\omega)$ as given by[49,50]

$$\alpha(\omega) = \sqrt{2}\omega\left[\sqrt{\epsilon'(\omega)^2+\epsilon''(\omega)^2} - \epsilon'(\omega)\right]^{1/2}. \quad (1)$$

Here, $\epsilon'(\omega)$ and $\epsilon''(\omega)$ are the real and imaginary part of the dielectric function $\epsilon(\omega)$ respectivity. The imaginary part $\epsilon''(\omega)$ is given by[49, 50]

$$\epsilon''(\omega) = \left(\frac{Ve^2}{2\pi\hbar m^2\omega^2}\right)\int d^3\boldsymbol{k}\sum_{nn'}|\langle \boldsymbol{kn}|\boldsymbol{p}|\boldsymbol{kn}'\rangle|^2 f(\boldsymbol{kn})$$
$$(1-f(\boldsymbol{kn}'))\delta(E_{\boldsymbol{kn}} - E_{\boldsymbol{kn}'} - \hbar\omega). \quad (2)$$

Here **p** is the momentum operator, $|\boldsymbol{kn}\rangle$ is the wave function, f(**kn**) denotes the Fermi function, and $\hbar\omega$ is the incident photon energy. After the imaginary part $\epsilon''(\omega)$ is known, the real part $\epsilon'(\omega)$ can be followed from the Kramers–Kronig relationship.

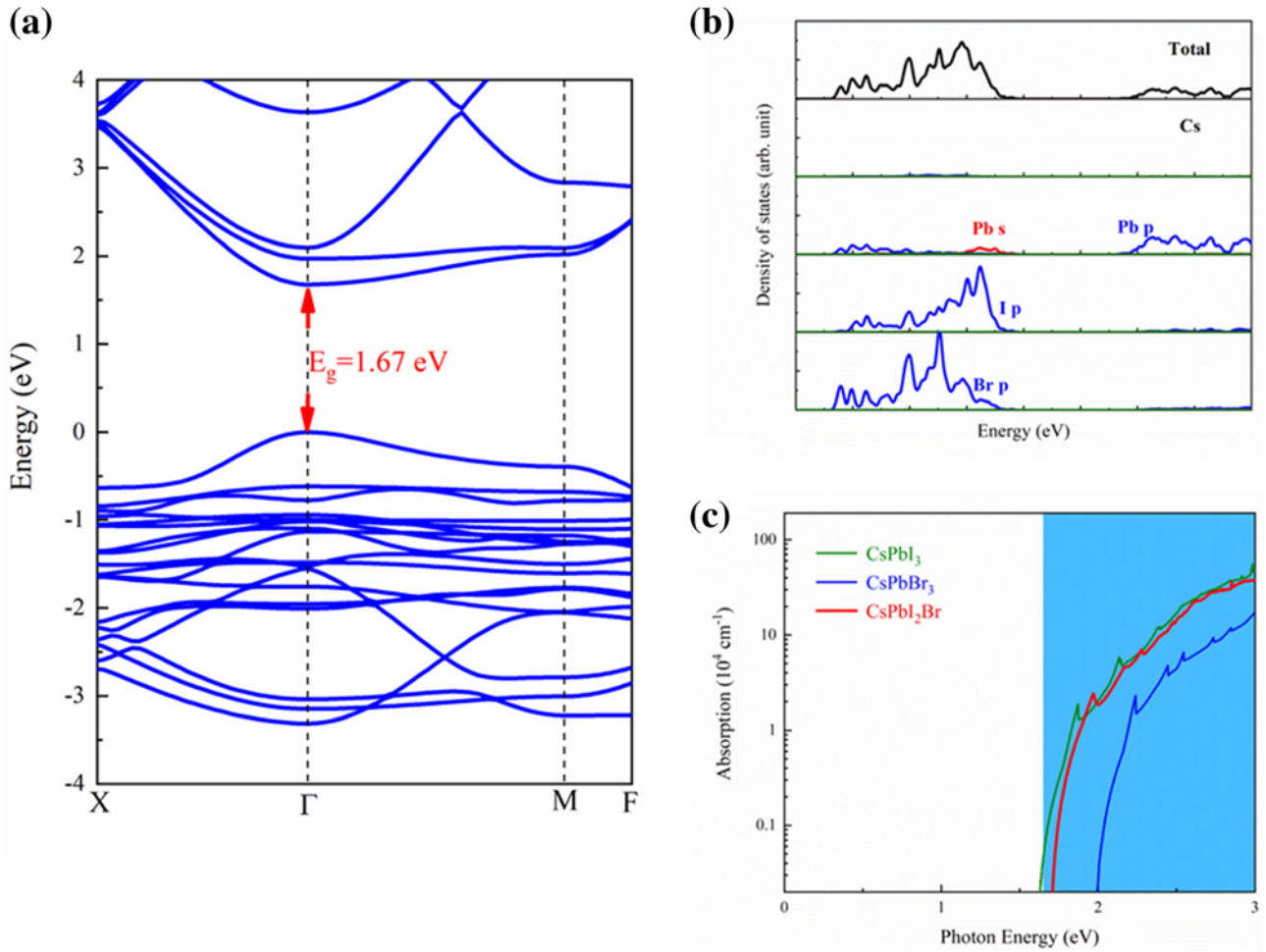

Figure 2. The PBE calculated (a) band structure, (b) projected density of states and (c) light absorption. The VBM energy in (a) and (b) is aligned to the zero energy. The blue region in the absorption curve (c) denotes the visible light range.

Following equation (1) and (2), the light absorption of the $CsPbI_2Br$ together with $CsPbBr_3$ and $CsPbI_3$ is shown in Figure 2(c). In the calculation, we have ensured the convergence of 9 × 9×9 k-point grid and the number of empty band states (twice NBANDS), and the test result has been also shown in Figure S2 (Supplementary Information). It is seen that their light absorption at the band gap edge raises rapidly up to above 10^4 cm^{-1}, and the light absorption in the visible light range (1.65–3.1 eV) is as strong as that of the popular $CH_3NH_3PbI_3$.[25] From Figure 2(c), comparing the light absorption of $CsPbI_2Br$ with that of the $CsPbBr_3$ and $CsPbI_3$, it is seen that the light absorption of $CsPbI_2Br$ is close to that of the $CsPbI_3$ but slightly stronger than that of the Br counterpart in the visible light range. The calculated light absorptions of $CsPbBr_3$ and $CsPbI_3$ are similar to the other reported results.[51] All of these electronic and optical properties show that $CsPbI_2Br$ is a good photovoltaic material.

3.3 *Band alignment*

In a heterojunction, the band alignment at the interface determines the charge transport properties at the interface. Appropriate energy level matching at the interface can contribute to the optimization of the solar cell.[27,28] The architecture of perovskite solar cell devices is usually classified into three types[33,52] that are defined by regular planar n-i-p, inverted planar p-i-n and mesoporous structures. For all of these structures, the extraction (injection) of electron and hole usually occur at the interface of perovskite/electron transport material (ETM) and perovskite/hole transport material (HTM), respectively. For perovskite solar cell devices, the commonly used ETM are ICBA, TiO_2, ZnO, SnO_2, PCBM and C_{60}, and the commonly used HTM are P3HT, CuI, NiO, PTAA and Spiro.[1,28,31,33,52] In general, in order to realize electron extraction efficiently, a proper band alignment of perovskite/ETM interface requires that the LUMO of ETM should be lower than

the CBM of the perovskite by about 0.2 eV.[30,31] On the other hand, to efficiently extract the holes and block the electrons, the HOMO of HTM should be slightly higher than the VBM of the perovskite.

The band alignment between different perovskites can also demonstrate the issues of doping level limit. As doping limit rule in the ref.[53,54] says "if the VBM is low, then it is difficult to dope to be p type, while if the CBM is high, then it is difficult to dope it to be n type". $CsPbI_2Br$ is a semiconductor that is mixed by the halide anion of $CsPbI_3$ and $CsPbBr_3$, understanding their tunable energy level variation is necessary. The calculation of the band alignment follows a well-defined computational procedure which is depicted in ref.[55,56]. In this procedure, the band alignment of the VBM between perovskite A and B can be defined as

$$\Delta E_v = \Delta E_{VBM,C}(A) - \Delta E_{VBM',C'}(B) + \Delta E_{C,C'} \quad (3)$$

here, the first term $(\Delta E_{VBM,C}(A) - \Delta E_{VBM',C'}(B))$ is the VBM energy difference between material A and B referred to each core level respectively. $\Delta E_{C,C'}$ is the core level (1 s) difference of the Cs atoms far away from the interface in a superlattice with 24 layers oriented in (001) direction. After the band alignment of the VBM is determined, then the band alignment of CBM can be directly obtained by plus the experimental band gap value of each perovskite (1.73 eV for $CsPbI_3$,[11,12] 2.3 eV for $CsPbBr_3$,[10,16] 1.92 eV for $CsPbI_2Br$[17–20] and 1.41 eV for $CsSnI_2Br$[57]). Following the equation (3), the band alignments between $CsPbI_2Br$ and $CsSnI_2Br$, $CsPbI_3$, $CsPbBr_3$ are obtained displayed in Figure 3(a). And the absolute energy levels (vs. vacuum level) of $CsPbI_3$ together with those ETM, HTM shown in Figure 3(a) are all directly extracted from the ref. [28,33] which are experimentally measured.

As seen in Figure 3(a), the band alignments between the commonly used ETM and $CsPbI_2Br$ show that the LUMO of TiO_2, ZnO, SnO_2, PCBM and C60 are all lower than the CBM of $CsPbI_2Br$, demonstrating that these ETM are also suitable for $CsPbI_2Br$ based solar cell devices. While the LUMO of ICBA is too high that would not be suitable for $CsPbI_2Br$ solar cell device. In the reported $CsPbI_2Br$ solar cells devices, the TiO_2 and SnO_2 are most frequently used,[21–23,32] and among those $CsPbI_2Br$ solar cells with the optimal parameter and high power transition efficiency,[32] the TiO_2 as ETM is the most favorite. Since the LUMO of ZnO and PCBM are close to that of the TiO_2 (< 0.1 eV), so the ZnO and PCBM served as ETM of $CsPbI_2Br$ based solar cell devices can also be a good choice. Moreover, the band alignments between the commonly used HTM and $CsPbI_2Br$ demonstrate that the HOMO of the P3HT, CuI, NiO, PTAA and Spiro are all higher than the VBM of the $CsPbI_2Br$, thus indicating all of them can be suitable HTM for $CsPbI_2Br$ solar cells. In reported $CsPbI_2Br$ solar cells with optimal parameters,[32] the HTM such as P3HT, PTAA and Spiro have frequently been used.[21–23, 32] In Figure 3(a), it is seen that the

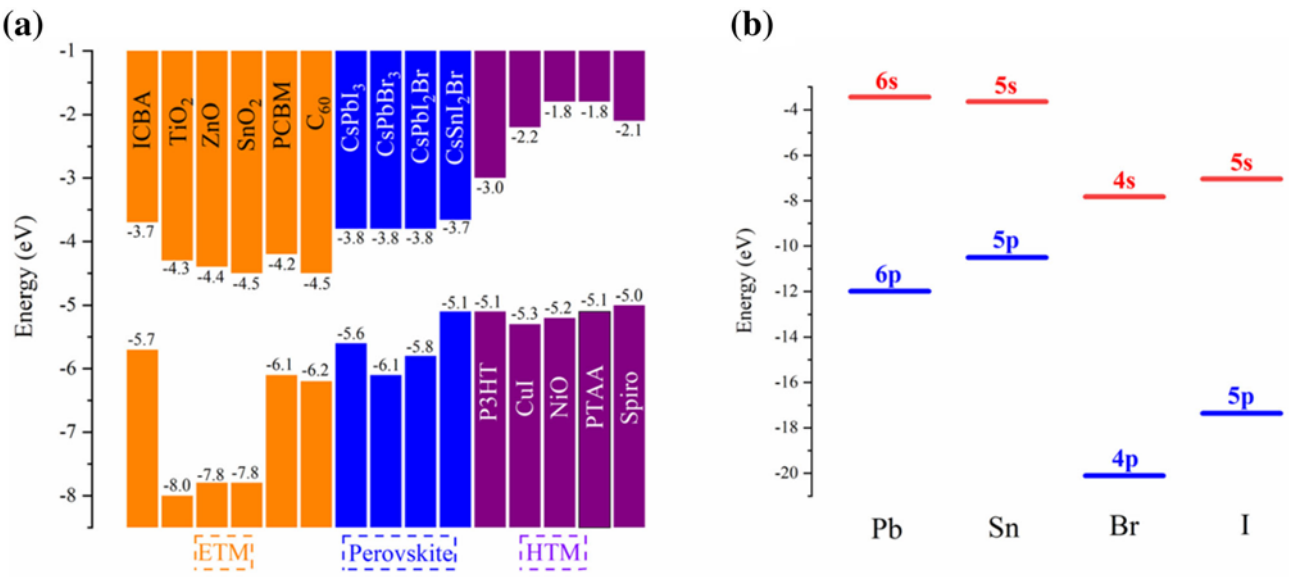

Figure 3. (a) Schematic energy levels of perovskites including $CsPbI_3$, $CsPbBr_3$, $CsPbI_2Br$ and $CsSnI_2Br$ together with the commonly used ETM (ICBA, TiO_2, ZnO, SnO_2, PCBM and C_{60}) and HTM (P3HT, CuI, NiO, PTAA and Spiro). Band alignments between different perovskites are calculated by equation (1), and the absolute energy levels of $CsPbI_3$ and the ETM, as well as the HTM, are all extracted from the ref. [28, 33]. The values of the absolute energy level for each material have been marked respectively. (b) PBE calculated valence atomic energy levels of Pb, Sn, Br and I.

HOMO of CuI and NiO are very close to that of P3HT, PTAA and Spiroframework of density functional theory, so CuI and NiO also could be good HTM for $CsPbI_2Br$ based solar cell devices.

As shown in Figure 3(a), $CsPbI_3$ has a higher VBM level and an equivalent height of CBM level compared to that of the $CsPbBr_3$. This can be understood by the analysis of their electronic structure and band components. Since the VBM of the $CsPbI_3$ and $CsPbBr_3$ are both derived from the antibonding states of the hybridization between Pb-s and halide-p states, so their relative height of VBM is mainly determined by the energy level of halide-p orbitals of the $CsPbI_3$ and $CsPbBr_3$. As diagrammatically displayed in Figure 3(b), we have calculated the energy levels of both s and p orbitals of Pb, Sn, Br and I, respectively. It can be seen that the atomic level of Br-p is lower than that of the I-p, accounting for the lower VBM of $CsPbBr_3$ than that of the $CsPbI_3$. According to the doping limit rule, the VBM of $CsPbBr_3$ is lower than that of the $CsPbI_3$, hence the $CsPbBr_3$ is more difficult to be doped p type than $CsPbI_3$. Despite the lower VBM of $CsPbBr_3$, the band gap of $CsPbBr_3$ (2.3 eV) is much larger than that of the $CsPbI_3$ (1.73 eV) thus making the CBM of $CsPbBr_3$ lie at the same height with that of the $CsPbI_3$. Similarly, the band alignment between $CsPbI_2Br$ and $CsPbI_3$ as well as $CsPbBr_3$ also can be understood. The $CsPbI_2Br$ has a VBM composed of Pb-s, I-p and Br-p, so the VBM level of $CsPbI_2Br$ is tuned to be higher than that of the $CsPbBr_3$ but lower than that of the $CsPbI_3$. After plus the band gap, the CBM of $CsPbI_2Br$ is same to that of the $CsPbI_3$ as well as the $CsPbBr_3$. The equivalent height of CBM level for them also can be understood by their uniform band component of CBM. As a lead free counterpart, the $CsSnI_2Br$ also has been attracted much attentions.[57–59] Since the energy level of Sn-p orbital is higher than that of the Pb-p orbital (see Figure 3(b)), so we can see that the CBM of $CsSnI_2Br$ is higher than that of the $CsPbI_2Br$. On the other hand, because the atomic radii of Sn is smaller than that of the Pb, hence the antibonding hybridization between the Sn-s and halide-p states are stronger thus pushing VBM upward and leading to a higher VBM of $CsSnI_2Br$ than that of the Pb counterpart. In consequence, according to the doping limit rule, the p-type doping for Pb-based perovskite is more difficult than that for Sn-based perovskite.

4. Conclusions

The all-inorganic perovskite $CsPbI_2Br$ has been considered as a very promising solar cell material with good stability as well as suitable bandgap. Through a first principles investigation on the electronic structure, optical properties and band alignments, we found that (i) the $CsPbI_2Br$ is stable in the tetragonal cell with a directbandgap of 1.67 eV under PBE calculations. The VBM is derived from the antibonding states of the hybridization between Pb-s states and halide-p states, and the CBM is mainly composed of Pb-p states; (ii) The optical absorption is as strong as above 10^4 cm^{-1} in the visual light range which can be comparable to that of the popular hybrid halide perovskites; (iii) The band alignments show that the commonly used ETM such as TiO_2, ZnO, SnO_2, PCBM and C_{60} and HTM such as P3HT, CuI, NiO, PTAA and Spiro in the popular perovskite solar cells are also suitable in the $CsPbI_2Br$ solar cells. The VBM of $CsPbI_2Br$ is higher than that of the $CsPbBr_3$ but lower than that of the $CsPbI_3$, while the CBM heights of them are equivalent. This demonstrates that it is easier for $CsPbI_2Br$ to be doped p type than that for $CsPbBr_3$ but more difficult than that for $CsPbI_3$.

5. Supplementary Information (SI)

The band structures of $CsPbI_2Br$ calculated by PBE + soc and hybrid + soc functional are given (Figure S1) available at www.ias.ac.in/chemsci.

Acknowledgements

This work was supported by National Natural Science Foundation of China (NSFC) under grant No. 61704097.

References

1. Shi J, Xu X, Li D and Meng Q 2015 Interfaces in perovskite solar cells *Small* **11** 2472
2. Burschka J, Pellet N, Moon S-J, Humphry-Baker R, Gao P, Nazeeruddin M K and Grätzel M 2013 Sequential deposition as a route to high-performance perovskite-sensitized solar cells *Nature* **499** 316
3. Yang W S, Park B-W, Jung E H, Jeon N J, Kim Y C, Lee D U, Shin S S, Seo J, Kim E K, Noh J H and Seok S I 2017 Iodide management in formamidinium-lead-halide–based perovskite layers for efficient solar cells *Science* **356** 1376
4. Moia D, Gelmetti I, Calado P, Fisher W, Stringer M, Game O, Hu Y, Docampo P, Lidzey D, Palomares E, Nelson J and Barnes P R 2019 Ionic-to-electronic current amplification in hybrid perovskite solar cells: ionically gated transistor-interface circuit model explains hysteresis and impedance of mixed conducting devices *Energy Environ. Sci.* **12** 1296

5. Kojima A, Teshima K, Shirai Y and Miyasaka T 2009 Organometal halide perovskites as visible-light sensitizers for photovoltaic cells *J. Am. Chem. Soc.* **131** 6050
6. Zhao D, Wang C, Song Z, Yu Y, Chen C, Zhao X, Zhu K and Yan Y 2018 Four-terminal all-perovskite tandem solar cells achieving power conversion efficiencies exceeding 23% *ACS Energy Lett.* **3** 305
7. Wang D, Wright M, Elumalai N K and Uddin A 2016 Stability of perovskite solar cells *Sol. Energy Mater. Sol. Cells* **147** 255
8. Conings B, Drijkoningen J, Gauquelin N, Babayigit A, D'Haen J, D'Olieslaeger L, Ethirajan A, Verbeeck J, Manca J, Mosconi E, Angelis F D and Boyen H-G 2015 Intrinsic thermal instability of methylammonium lead trihalide perovskite *Adv. Energy Mater.* **5** 1500477
9. Liang J, Liu J and Jin Z 2017 All-inorganic halide perovskites for optoelectronics: progress and prospects *Sol. RRL* **1** 1700086
10. Liang J, Wang C, Wang Y, Xu Z, Lu Z, Ma Y, Zhu H, Hu Y, Xiao C, Yi X, Zhu G, Lv H, Ma L, Chen T, Tie Z, Jin Z and Liu J 2016 All-inorganic perovskite solar cells *J. Am. Chem. Soc.* **138** 15829
11. Eperon G E, Paternò G M, Sutton R J, Zampetti A, Haghighirad A A, Cacialli F and Snaith H J 2015 Inorganic caesium lead iodide perovskite solar cells *J. Mater. Chem. A* **3** 19688
12. Stoumpos C C, Malliakas C D and Kanatzidis M G 2013 Semiconducting tin and lead iodide perovskites with organic cations: phase transitions, high mobilities, and near-infrared photoluminescent properties *Inorg. Chem.* **52** 9019
13. Wang Q, Jin Z, Chen D, Bai D, Bian H, Sun J, Zhu G, Wang G and Liu S 2018 μ-graphene crosslinked $CsPbI_3$ quantum dots for high efficiency solar cells with much improved stability *Adv. Energy Mater.* **8** 1800007
14. Sanehira E M, Marshall A R, Christians J A, Harvey S P, Ciesielski P N, Wheeler L M, Schulz P, Lin L Y, Beard M C and Luther J M 2017 Enhanced mobility $CsPbI_3$ quantum dot arrays for record-efficiency, high-voltage photovoltaic cells *Sci. Adv.* **3** eaao4204
15. Wang Q, Zheng X, Deng Y, Zhao J, Chen Z and Huang J 2017 Stabilizing the α-phase of $CsPbI_3$ perovskite by sulfobetaine zwitterions in one-step spin-coating films *Joule* **1** 371
16. Akkerman Q A, Gandini M, Stasio F D, Rastogi P, Palazon F, Bertoni G, Ball J M, Prato M, Petrozza A and Manna L 2016 Strongly emissive perovskite nanocrystal inks for high-voltage solar cells *Nat. Energy* **2** 16194
17. Wang Y, Zhang T, Xu F, Li Y and Zhao Y 2018 A facile low temperature fabrication of high performance $CsPbI_2Br$ all-inorganic perovskite solar cells *Sol. RRL* **2** 1700180
18. Beal R E, Slotcavage D J, Leijtens T, Bowring A R, Belisle R A, Nguyen W H, Burkhard G F, Hoke E T and McGehee M D 2016 Cesium lead halide perovskites with improved stability for tandem solar cells *J. Phys. Chem. Lett.* **7** 746
19. Mariotti S, Hutter O S, Phillips L J, Yates P J, Kundu B and Durose K 2018 Stability and performance of $CsPbI_2Br$ thin films and solar cell devices *ACS Appl. Mater. Inter.* **10** 3750
20. Liu C, Li W, Zhang C, Ma Y, Fan J and Mai Y 2018 All-inorganic $CsPbI_2Br$ perovskite solar cells with high efficiency exceeding 13% *J. Am. Chem. Soc.* **140** 3825
21. Tian J, Xue Q, Tang X, Chen Y, Li N, Hu Z, Shi T, Wang X, Huang F, Brabec C J, Yip H L and Cao Y 2019 Dual interfacial design for efficient $CsPbI_2Br$ perovskite solar cells with improved photostability *Adv. Mater.* **31** 1901152
22. Wang K L, Wang R, Wang Z K, Li M, Zhang Y, Ma H, Liao L S and Yang Y 2019 Tailored phase transformation of $CsPbI_2Br$ films by copper(II) bromide for high-performance all-inorganic perovskite solar cells *Nano Lett.* **19** 5176
23. Chen W, Chen H, Xu G, Xue R, Wang S, Li Y and Li Y 2019 Precise control of crystal growth for highly efficient $CsPbI_2Br$ perovskite solar cells *Joule* **3** 191
24. Jono R and Segawa H 2019 Theoretical study of the band-gap differences among lead triiodide perovskite materials: $CsPbI_3$, $MAPbI_3$, and $FAPbI_3$ *Chem. Lett.* **48** 877
25. Yin W-J, Shi T and Yan Y 2014 Unique properties of halide perovskites as possible origins of the superior solar cell performance *Adv. Mater.* **26** 4653
26. Huang Y, Yin W-J and He Y 2018 Intrinsic point defects in inorganic cesium lead iodide perovskite $CsPbI_3$ *J. Phys. Chem. C* **122** 1345
27. Feng W, Rangan S, Cao Y, Galoppini E, Bartynski RA and Garfunkel E 2014 Energy level alignment of polythiophene/ZnO hybrid solar cells *J. Mater. Chem. A* **2** 7034
28. Yang Z, Dou J and Wang M 2018 Interface engineering in n-i-p metal halide perovskite solar cells *Sol. RRL* **2** 1800177
29. Schulz P, Edri E, Kirmayer S, Hodes G, Cahen D and Kahn A 2014 Interface energetics in organo-metal halide perovskite-based photovoltaic cells *Energy Environ. Sci.* **7** 1377
30. Park N-G 2013 Organometal perovskite light absorbers toward a 20% efficiency low-cost solid-state mesoscopic solar cell *J. Phys. Chem. Lett.* **4** 2423
31. Zhou Z, Pang S, Liu Z, Xu H and Cui G 2015 Interface engineering for high-performance perovskite hybrid solar cells *J. Mater. Chem. A* **3** 19205
32. Zeng Q, Zhang X, Liu C, Feng T, Chen Z, Zhang W, Zheng W, Zhang H and Yang B 2019 Inorganic $CsPbI_2Br$ perovskite solar cells: the progress and perspective *Sol. RRL* **3** 1800239
33. Bai Y, Meng X and Yang S 2018 Interface engineering for highly efficient and stable planar p-i-n perovskite solar cells *Adv. Energy Mater.* **8** 1701883
34. Yin W-J, Shi T and Yan Y 2014 Unusual defect physics in $CH_3NH_3PbI_3$ perovskite solar cell absorber *Appl. Phys. Lett.* **104** 063903
35. Kresse G and Furthmüller J 1996 Efficiency of ab-initio total energy calculations for metals and semiconductors using a plane-wave basis set *Comp. Mater. Sci.* **6** 15
36. Kresse G and Furthmüller J 1996 Efficient iterative schemes for ab initio total-energy calculations using a plane-wave basis set *Phys. Rev. B* **54** 11169
37. Blöchl P E 1994 Projector augmented-wave method *Phys. Rev. B* **50** 17953

38. Kresse G and Joubert D 1999 From ultrasoft pseudopotentials to the projector augmented-wave method *Phys. Rev. B* **59** 1758
39. Perdew J P, Burke K and Ernzerhof M 1996 Generalized gradient approximation made simple *Phys. Rev. Lett.* **77** 3865
40. Yin W-J, Yan Y and Wei S-H 2014 Anomalous alloy properties in mixed halide perovskites *J. Phys. Chem. Lett.* **5** 3625
41. Magri R, Wei S H and Zunger A 1990 Ground-state structures and the random-state energy of the Madelung lattice *Phys. Rev. B* **42** 11388
42. Wei S H, Ferreira L G, Bernard J E and Zunger A 1990 Electronic-properties of random alloys - special quasirandom structures *Phys. Rev. B* **42** 9622
43. Wei S H, Ferreira L G and Zunger A 1990 1st-principles calculation of temperature-composition phase-diagrams of semiconductor alloys *Phys. Rev. B* **41** 8240
44. Zunger A, Wei S H, Ferreira L G and Bernard J E 1990 Special quasirandom structures *Phys. Rev. Lett.* **65** 353
45. Mosconi E, Amat A, Nazeeruddin M K, Grätzel M and Angelis F D 2013 First-principles modeling of mixed halide organometal perovskites for photovoltaic applications *J. Phys. Chem. C* **117** 13902
46. Li Y, Zhang C, Zhang X, Huang D, Shen Q, Cheng Y and Huang W 2017 Intrinsic point defects in inorganic perovskite $CsPbI_3$ from first-principles prediction *Appl. Phys. Lett.* **111** 162106
47. Heyd J, Scuseria G E and Ernzerhof M 2003 Hybrid functionals based on a screened Coulomb potential *J. Chem. Phys.* **118** 8207
48. Paier J, Marsman M, Hummer K, Kresse G, Gerber I C and Ángyán J G 2006 Screened hybrid density functionals applied to solids *J. Chem. Phys.* **124** 154709
49. Ravindran P, Delin A, Johansson B, Eriksson O and Wills J M 1999 Electronic structure, chemical bonding, and optical properties of ferroelectric and antiferroelectric $NaNO_2$ *Phys. Rev. B* **59** 1776
50. Saha S, Sinha T P and Mookerjee A 2000 Electronic structure, chemical bonding, and optical properties of paraelectric $BaTiO_3$ *Phys. Rev. B* **62** 8828
51. Murtaza G and Ahmad I 2011 First principle study of the structural and optoelectronic properties of cubic perovskites $CsPbM_3$ (M = Cl, Br,I) *Physica B* **406** 3222
52. Da P, Zheng G 2017 Tailoring interface of lead-halide perovskite solar cells *Nano Res.* **10** 147152
53. Wei S-H 2004 Overcoming the doping bottleneck in semiconductors *Comp. Mater. Sci.* **30** 337
54. Zhang S B, Wei S-H and Zunger A 1999 Overcoming doping bottlenecks in semiconductors and wide-gap materials *Physica B* **273** 976
55. Wei S-H and Zunger A 1987 Role of d orbitals in valence-band offsets of common-anion semiconductors *Phys. Rev. Lett.* **59** 144
56. Wei S-H and Zunger A 1988 *Role of d Orbitals in Valence-Band Offsets of Common-Anion Semiconductors. In: Electronic Structure of Semiconductor Heterojunctions* G Margaritondo (Ed.) (Dordrecht: Springer Netherlands) p. 200
57. Peedikakkandy L and Bhargava P 2016 Composition dependent optical, structural and photoluminescence characteristics of cesium tin halide perovskites *RSC Adv.* **6** 19857
58. Sabba D, Mulmudi H K, Prabhakar R R, Krishnamoorthy T, Baikie T, Boix P P, Mhaisalkar S and Mathews N 2015 Impact of anionic Br–substitution on open circuit voltage in lead free perovskite ($CsSnI_{3-x}Br_x$) solar cells *J. Phys. Chem. C* **119** 1763
59. Varadwaj A, Varadwaj P R and Yamashita K 2018 Revealing the chemistry between band gap and binding energy for lead-/tin-based trihalide perovskite solar cell semiconductors *ChemSusChem* **11** 449